*Proceedings of the 21st ICSMGE, Vienna, Austria, 14 – 19 June 2026. Pistrol, Adam & Schweiger (eds.)*
*Published by: ÖGG, Austrian Society for Geomechanics, Salzburg, Austria, ISBN 978-3-9503898-4-5*
*https://doi.org/10.53243/ICSMGE2026-1367*

# On the comparison of the performance of different liquefaction constitutive models and pore water pressure generation methods: The Gölbaşı-Türkiye case study

**Sinan Sargin,** Guldem Korkmaz, Emirhan Altinok, Sadik Oztoprak, M. Kubilay Kelesoglu, İlknur Bozbey
*Istanbul University-Cerrahpasa, Istanbul, Turkiye, ssargin@iuc.edu.tr*

Ahmet Kaan Yildirim,
*Istanbul Nisantasi University, Istanbul, Türkiye*

Fatma Tuğçe Cinar Ozkan,
*Kahramanmaras Sutcu Imam University, Kahramanmaras, Türkiye*

ABSTRACT: On February 6, 2023, two powerful earthquakes (Mw 7.7 and Mw 7.6) struck southeastern Türkiye within nine hours, with epicenters in the Pazarcık and Elbistan districts of Kahramanmaraş. The earthquakes caused widespread damage due to ground deformations, soil failures, and structural deficiencies. Notably, soil liquefaction-related damage was concentrated in Gölbaşı district, Adıyaman, drawing significant research attention. This study examines liquefaction in Gölbaşı from a site response perspective. As part of a research project funded by the Scientific and Technological Research Council of Türkiye, comprehensive geotechnical site investigations were conducted, including laboratory tests on disturbed and undisturbed soil samples. A representative soil profile was developed using in-situ and laboratory test results. In the first phase, one-dimensional (1-D) site response analyses were performed on this profile using earthquake records with varying characteristics. In the second phase, excess pore water pressure (EPWP) generation, a key factor triggering soil liquefaction, was modeled using nonlinear analyses in DeepSoil software. These analyses were validated through simulations in Plaxis 2D using advanced constitutive models (UBC3D-PLM, PM4Sand, PM4Silt) for soil liquefaction. The study presents a comparative analysis of EPWP development in soils prone to liquefaction and cyclic mobility, emphasizing critical considerations in applying constitutive models and selecting parameters. The findings provide valuable insights for improving disaster preparedness and response strategies, both in Türkiye and globally.

KEYWORDS: Liquefaction, 1D site response, UBC3D-PLM, PM4Silt, PM4Sand, Kahramanmaraş Earthquakes, Gölbaşı-Türkiye

## 1 INTRODUCTION

The February 6, 2023 earthquakes in southeastern Türkiye caused widespread damage, with soil liquefaction effects particularly evident in the Gölbaşı district of Adıyaman. The earthquake, registering a magnitude of 7.8, resulted in extensive devastation in the affected regions, leading to tens of thousands of fatalities, displacing millions, and reducing numerous buildings to rubble. The seismic event occurred at 4:17 AM local time (01:17 UTC) on February 6, 2023, with its epicenter located near the city of Gaziantep in southern Türkiye. This earthquake was attributed to tectonic activity along the East Anatolian Fault (EAF), a significant strike-slip fault traversing the region (Arpat & Şaroğlu, 1972).

In the aftermath of the earthquake, extensive reconnaissance field investigations were conducted in the affected region. The February 2023 Kahramanmaraş earthquakes inflicted substantial damage in southeastern Türkiye, notably causing significant soil liquefaction in the Gölbaşı district of Adıyaman (Tonyalı et al., 2024;Flora et al.; Özden & Kartal, 2025). This is closely related with the geology of the area. Akıl et al. (2008) demonstrated that a substantial portion of the settlement area consists of Quaternary alluvial geological formations. The region surrounding Lake Gölbaşı, located to the north of the Malatya-Maraş Road, contains lake alluvium and swamp sediments, which bisect the district Manifestation of liquefaction was documented in various soil types, including clayey sands and even some high-plasticity clays (Cetin et al., 2024). The seismic events led to surface ruptures, lateral spreading, and ground deformations in the impacted areas (Gokceoglu, 2023; Sandıkçıoğlu et al., 2023). Geotechnical investigations indicated that certain areas of Kahramanmaraş city exhibited a high potential for liquefaction even prior to the 2023 events (Cabalar et al., 2019). The earthquakes also affected industrial facilities, resulting in liquefaction-induced damage to petrochemical plants (Şahin & Cetin, 2024). Post-earthquake analyses revealed that while predictions of liquefaction triggering were generally accurate, existing methods frequently underestimated settlements and overestimated lateral displacements in certain soil types (Şahin & Cetin, 2024; Milev et al., 2024).

Öser et al. (2024) reported that extensive ground settlements resulting from liquefaction were observed in Gölbaşı following the earthquakes on February 6, 2023. These settlements were particularly pronounced in regions characterized by alluvial fill, where surface fissures and structural tilting were common. The authors highlighted that the shallow groundwater table played a significant role in diminishing the bearing capacity, thereby adversely affecting building performance.

This study investigates the effects of liquefaction on site response analysis in Gölbaşı based on a representative soil profile. The aim is to understand the development of excess pore water pressure in liquefiable soils, emphasizing key considerations for the application of constitutive models and the selection of parameters. A comprehensive geotechnical investigation study was conducted as a part of TÜBİTAK, The Scientific and Technological Research Council of Türkiye) funded (Bozbey et al.2023) research project for site chatacterization. One-dimensional site response analyses were performed using an earthquake record located approximately 30 km away. Excess pore water pressure generation was subsequently modeled using nonlinear analyses in DeepSoil (Hashash, 2020) and validated through simulations in Plaxis 2D (Bentley, 2025) with advanced constitutive models for soil liquefaction. The findings aim to enhance the understanding of liquefaction behavior and inform disaster preparedness strategies.

## 2 SITE CHARACTERIZATION

In order to characterize the soil layers at the study site, Cone Penetration Test (CPT), Standard Penetration Test (SPT), and geophysical field tests Multichannel Analysis of Surface Waves (MASW) and Spatial Auto Correlation Method (SPAC) were carried out.

Figure 1(a) and Figure 1(b) present the depth–tip resistance (qc) and depth–sleeve friction (fs) profiles obtained from a typical CPT sounding carried out in the area. In Figure 1(c), the Soil Behavior Type Index (IC), calculated based on qc and fs according to Robertson (2009), is presented. Based on the Ic values, the upper 8.5 m layer was classified as silty clay, while the layer between 8.5 m and 12.5 m exhibited silty sand characteristics. Figure 1(d) illustrates the stratigraphy and SPT results obtained from borehole drilling at the site. The groundwater table was identified at an approximate depth of 2.0 m. $N_{1,60}$ values ranged between 5 and 10 within the first 8 m, and showed a noticeable increase beyond 8 m depth. Overall, the borehole observations which defined the soil as silty clays and clayey sands, were found to be in good agreement with the Ic-based classifications. The laboratory index testing carried out on disturbed and undisturbed samples indicated that the soil profile up to a depth of 20 m generally consists of a clayey sand–clay mixtures. Figure 2 presents the depth–average shear wave velocity (VS) profiles obtained from SPAC and MASW tests. According to these results, the engineering bedrock (VS > 760 m/s) was encountered at an approximate depth of 190 m. The shear waves were significantly lower than 300 m/s in the first 30 meters.

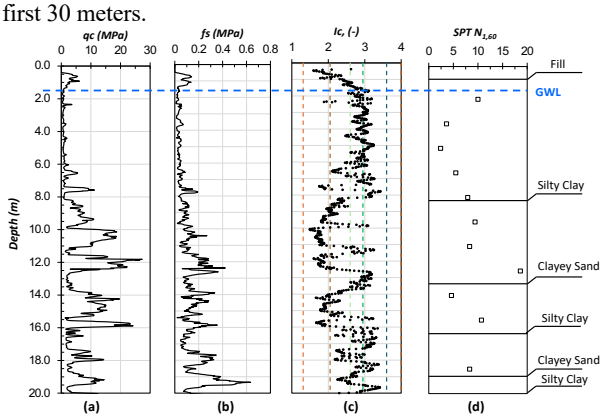


Figure 1. Field test results: (a) cone resistance, (b) sleeve friction, (c) Soil Behavior Index (Robertson,2009) with depth based on CPT; (d) Corrected SPT blow numbers with depth (Bozbey et al.,2023)

Some of the CPT soundings performed in this study, pore water pressure values lower than the hydrostatic (phreatic) levels were measured. This atypical response is thought to result from the presence of gravel-rich lenses embedded between the clayey and sandy strata, which may create localized drainage paths and reduce measured pore pressures.

USCS classifications show that the upper 3–5 m of the subsurface generally consists of clayey sands (SC) in most boreholes. Thin layers of low-plasticity clay (CL) also appear intermittently within this zone. The combination of SC, CL, and CH units highlights the strong influence of fines content on excess pore pressure development throughout the soil profile, although occasional coarse-grained interbeds are present. Well-graded sandy layers, with or without silt and clay (SW, SW-SM, SP-SM) were identified in only a few isolated locations. When evaluated against the particle-size boundaries proposed by Tsuchida (1970), many of these soils exhibit characteristics that were not consistent with liquefaction-susceptible profiles. Nearly all the sampled fine-grained soils plot outside Zone A, (potentially susceptible to classic cyclically induced liquefaction), while majority of the samples lie in Zone B (encompasses intermediate soils that occupy a transitional region) and Zone C (generally not susceptible to classic cyclically induced soil liquefaction) of the Seed et al. (2003) liquefaction-susceptibility criteria. This distribution indicates that only a limited subset of the materials satisfies the conditions for potential liquefaction, whereas cyclic softening is likely the governing seismic response mechanism for the majority of the deposits.

## 3 NUMERICAL ANALYSIS

To perform one-dimensional site response analyses that take into account the liquefaction potential of the soils in Gölbaşı, it was necessary to obtain a reliable ground motion record from a station near to the site. For this purpose, the N–S component of the TK-4611 Çağlayancerit station (approximately 32 km.) record, associated with the Mw 7.7 mainshock of the February 6 earthquakes and provided by AFAD (2025), was employed (Figure 3).

To simulate the conditions of liquefaction or cyclic mobility induced by earthquake-generated excess pore water pressure in Gölbaşı during the February 6 earthquakes, five distinct analytical scenarios were developed utilizing two different software tools. As summarized in Table 1, the analyses were conducted using DeepSoil (Hashash et al., 2020) and Plaxis 2D (Bentley, 2025).

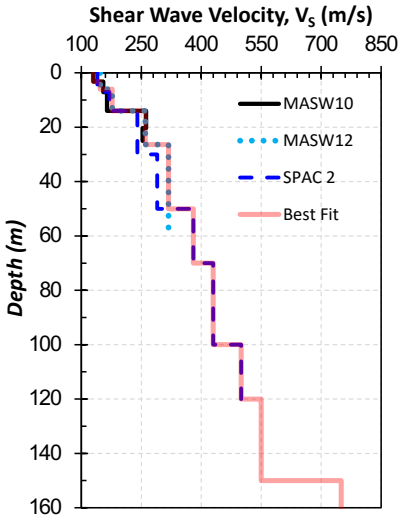


Figure 2. Shear wave velocity (Vs) profiles obtained from in-situ geophysical tests (MASW10, MASW12, SPAC2), along with the best-fit model (Bozbey et al., 2023).

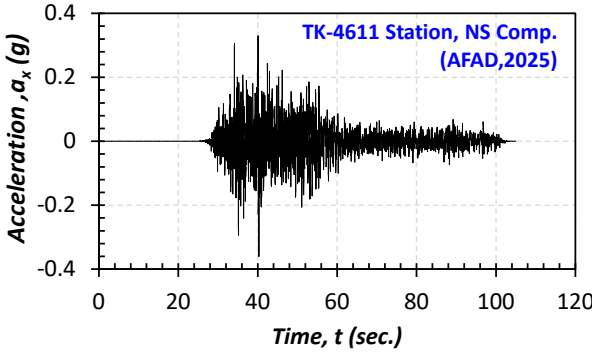


Figure 3. Strong ground motion record used as input motion for analysis (AFAD, 2025)

Liquefiable soil layers were identified within the upper 20 meters based on CPT data, where the factor of safety against liquefaction was found to be less than 1.0 according to the procedure proposed by Boulanger and Idriss (2014). At greater

depths, due to elevated shear wave velocity values, the soil was assumed to be non-liquefiable.

The nonlinear analysis option in the DeepSoil software, which is capable of generating excess pore water pressure, was utilized.

Table 1. Summary of the Analyses

| Analysis No | Software | Explanation |
|---|---|---|
| 1 | Plaxis2D-Site Respone Module | PM4Sand and PM4Silt constitutive model for liquefiable layers, HSSmall for non-liquefiable layers |
| 2 | | PM4Sand and PM4Silt constitutive model for liquefiable layers, Linear Elastic model for non-liquefiable layers |
| 3 | | UBC3D-PLM constitutive model for liquefiable layers, HSSmall for non-liquefiable layers |
| 4 | | UBC3D-PLM constitutive model for liquefiable layers, Linear Elastic model for non-liquefiable layers |
| 5 | DeepSoil | Nonlinear Analysis with excess pore water pressure with MRD curves |

For this purpose, the pore pressure generation models available in DeepSoil, as proposed by Matasovic and Vucetic (1993,1995) for granular soils and by Matasovic (1995) for cohesive soils, whose mathematical expressions are provided in Equation (1) and (2), were calibrated using Cyclic Direct Simple Shear (CDSS) tests conducted on reconstituted soil samples collected from the field, as depicted in Figure 4(a) and 4(b), respectively. The calibrated model parameters are presented in Table 2. Additionally, for modulus reduction and damping (MRD) curves, the models proposed by Menq (2003) for granular soils and by Darendeli (2001) for cohesive soils were adopted.

$$u_N = \frac{p * f * N_C * F * (\gamma_c - \gamma_{tvp})^s}{1 + f * N_C * F * (\gamma_c - \gamma_{tvp})^s} \quad (1)$$

$$u_N = A{N_C}^{-3s(\gamma_c - \gamma_{tvp})^r} + B{N_C}^{-2s(\gamma_c - \gamma_{tvp})^r} + C{N_C}^{-s(\gamma_c - \gamma_{tvp})^r} + D \quad (2)$$

Table 2. The parameters of the calibrated models proposed by Matasovic/Dobry (1993,1995) and Matasovic (1995)

| Parameter | Value | Description |
|---|---|---|
| $u_N$ | - | Excess pore water pressure (EPWP) ratio |
| $N_{eq}$ | from tests | Equivalent number of cycles |
| $\gamma_c$ | from tests | The current reversal shear strain |
| $\gamma_{tvp}$ | 0.01 | Threshold shear strain to generate EPWP |
| p, s, F, f | 1.1,1.0,8.0, 1.0 | Curve fitting and adjustment parameters for Dobry/Matasovic model (1992,1993) |
| s, r, A, B, C, D | 0.21,0.3,7.7, - 14.7,6.5,0.8 | Curve fitting and adjustment parameters for Matasovic model (1995) |

In one-dimensional site response analyses conducted using Plaxis 2D (Bentley, 2025), CPT and SPT data, given in Figure 1, were employed to define the soil stratigraphy and input parameters. To model liquefaction or cyclic mobility behavior, the PM4Sand V3.3 (Boulanger & Ziotopoulou, 2023) constitutive model was utilized for silty sands with high fines content (FC:20–30%).

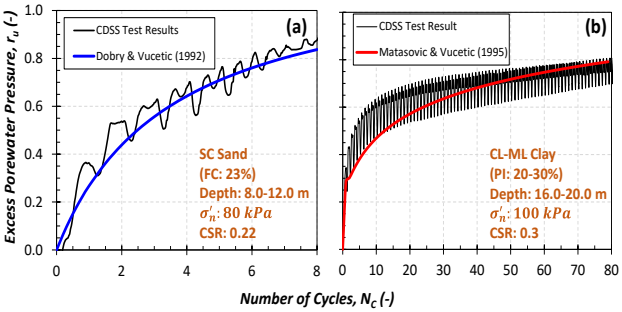


Figure 4. Calibration of pore pressure model embedded in DeepSoil with cyclic direct simple shear test results: (a) Fine Sand, (b) Silty Clay (Bozbey et al.,2023)

Furthermore, significant liquefaction potential, whereas the PM4Silt (Boulanger & Ziotopoulou, 2023) model was applied to low-plasticity clayey and silty layers. For the calibration of both models, the results of Cyclic Direct Simple Shear (CDSS) tests were simulated in Soiltest Module of the software, as illustrated in Figure 5 (a) and (b), and the experimental liquefaction resistance curves (LRC) presented in Figure 5(c) were accurately reproduced. The primary parameters of the constitutive models for calibration were presented in Table 3 and 0, respectively. In this study, the secondary parameters were maintained at their default values, in accordance with the recommendations of Boulanger and Ziotopoulou, with the exception of $C_\varepsilon$, which was modified for a minor adjustment.

Table 3. The key parameters of PM4Sand used in model)

| Parameter | Layers with depth | | |
|---|---|---|---|
| | L1 (z=0.0-1.5m) | L4 (z=8.5-12.5m) | L6 (z=14.5-16.5m) |
| $D_{R,0}$ | 0.5 | 0.45 | 0.47 |
| $G_0$ | 729 | 556 | 687 |
| $h_{p,0}$ | 0.1 | 7.0 | 3.5 |

Where $D_{R0}$ denotes the initial relative density controlling the sand's state parameter and dilatancy behavior, $G_0$ represents the small-strain shear modulus defining the initial stiffness of the soil skeleton, and $h_{p0}$ is the contractive parameter governing the rate of pore pressure generation during cyclic loading

Table 4. The key parameters of PM4Silt used in model

| Parameter | Layers with depth | | | |
|---|---|---|---|---|
| | L2 (z=1.5-4.5m) | L3 (z=4.5-8.5m) | L5 (z=12.5-14.5m) | L7 (z=16.5-20.5m) |
| $s_u$ (kPa) | 50 | 55 | 70 | 60 |
| $G_0$ | 576 | 600 | 1258 | 978 |
| $h_{p,0}$ | 10 | 10 | 1.0 | 1.8 |
| $c_\varepsilon$ | 0.85 | 0.85 | 1.25 | 0.65 |

Here $S_{u0}$ denotes the undrained shear strength defining the initial yield resistance of the cohesive soil, $G_0$ represents the small-strain shear modulus controlling the initial stiffness of the soil skeleton, $h_{p0}$ is the contractive parameter influencing the rate of excess pore pressure generation under cyclic loading, And $C_\varepsilon$ defines the rate of shear strain accumulation and governs the strain-dependent damping behavior of the soil under cyclic loading.

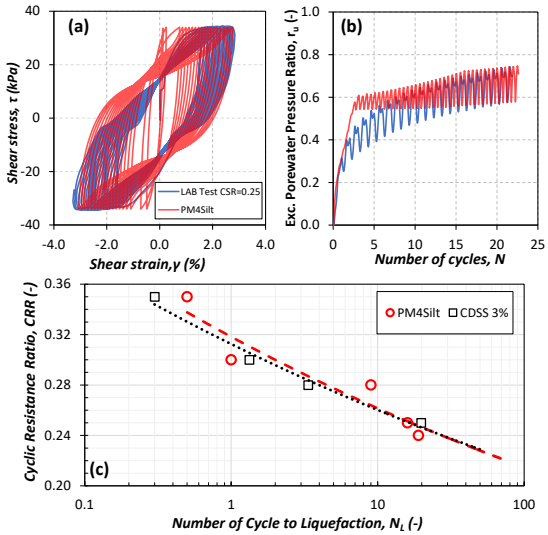


Figure 5. Schematic illustration of the PM4Silt model calibration and validation in Plaxis 2D using the SoilTest toolbox, including cyclic hysteresis loops (CSR = 0.25) and excess pore pressure ratio evolution. Comparison with experimental liquefaction resistance curves (3% SA shear strain) (Bozbey et al., 2023).

In the calibration process of UBC3D-PLM, the model parameters are based on N-SPT values. Revised (Makra, 2013) version of the proposed Equations(3)-(7) for the generic initial calibration are the following:

$$\phi_p = \phi_{cv} + \frac{N_{1,60}}{10} + max\,(0; \frac{N_{1,60} - 15}{5}) \quad (3)$$

$$K_G^e = 21.7 \cdot 20 \cdot (N_{1,60})^{0.3333} \quad (4)$$

$$K_B^e = 0.7 \cdot K_G^e \quad (5)$$

$$K_G^p = K_G^e \cdot (N_{1,60})^2 \cdot 0.003 + 100 \quad (6)$$

$$R_f = 1.1 \cdot (N_{1,60})^{-0,15} \quad (7)$$

In this context, $\phi_p$ represents the peak friction angle, while $\phi_{cv}$ denotes the friction angle at constant volume. The elastic shear modulus, plastic shear modulus, and elastic bulk modulus are also considered. The failure ratio is indicated by $R_f$. The corrected SPT values ($N_{1,60}$) for layers L1, L4, and L6 are initially defined as 9, 13.2, and 10, respectively. The remaining soil layers are identified as non-liquefiable and are modeled using the HSSmall constitutive model (Bentley, 2025) which facilitates the analysis of soil behavior within a small-to-medium strain range. Consequently, the compatibility between liquefiable and non-liquefiable layers is ensured.

In the dynamic analyses of the soil column conducted using the 'site response' feature in Plaxis2D, the model's lower boundary was designated as a "compliant base," while the lateral boundaries were assigned boundary conditions with "tied degrees of freedom". To achieve a target damping ratio of 2% at small strain levels, the Rayleigh damping coefficients were determined as α = 0.2633 and β = 0.625E-3. These coefficients were calculated considering the soil's fundamental frequency of 1.186 Hz and the ratio of 9 between this frequency and the frequency corresponding to the peak amplitude of the input motion.

## 4 RESULTS

This section delineates the principal findings obtained from the analyses conducted. The results present the shear strain, horizontal maximum acceleration and pore pressure ratio values versus depth. The constitutive model used in analyses within depth is also presented

Figure 6(a) demonstrates that significant shear strains have developed within the upper 5 meters of the soil profile, particularly in Analyses No.1 and No.5.). This observation suggests the presence of highly deformable or potentially liquefiable soil layers near the surface. Furthermore, Figure 6(b) illustrates that horizontal maximum acceleration values are amplified in the upper layers, with distinct peaks observed in Analyses No.3 and No.5, underscoring the influence of soft soils on seismic wave amplification. Additionally, Figure 6(c) indicates that the excess pore pressure ratio ($r_u$) approached unity at certain depths in Analyses No.1 and No.5, signifying a high potential for liquefaction or cyclic mobility under seismic loading.

In light of the depth-dependent variation in both maximum acceleration and excess pore pressure ratio, the shear stress–shear strain behavior was analyzed at a depth of 3 meters, which is representative of the typical foundation depth for conventional reinforced concrete buildings in Gölbaşı.

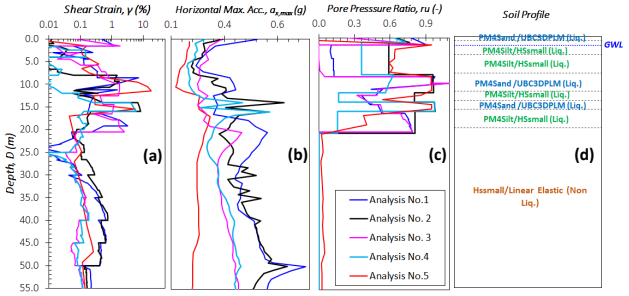


Figure 6. Analysis Results a) Shear Strain, b) Max. Acceleration, c) Max. Pore pressure, d) Constitutive Models with depth

For a more precise comparison, the results of the analyses utilizing MRD curves for soil layers modeled from a depth of 20 meters and below are presented in Figure 7(a), (b), and (c). Figure 7(a) shows pronounced nonlinear behavior and energy dissipation at 3 meters depth, suggesting cyclic mobility or early liquefaction. In contrast, Figure 7(b) and (c), representing deeper layers with MRD modeling, exhibit narrower, more stable loops indicative of elastic or slightly nonlinear soil response. These results highlight the increased relevance of MRD-based modeling at greater depths.

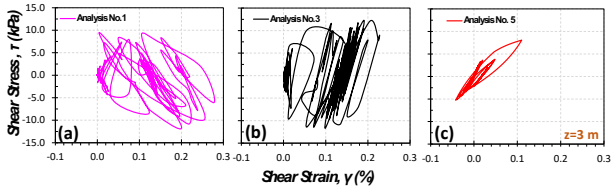


Figure 7. Shear stress-strain results obtained from MRD curves considered NL analyses

The analyses in which soil layers located below the initial 20 meters were modeled using a linear elastic approach—without allowing for modulus reduction or hysteretic damping—are compared in Figure 8(a) and (b). Figure 8(a) demonstrates that the soil response at deeper layers, modeled with a linear elastic approach without accounting for modulus reduction or hysteretic damping, exhibits limited nonlinear behavior and low energy dissipation. In contrast, Figure 8(b) shows a much wider hysteresis loop at a depth of 3 meters, indicating significant nonlinear deformation and cyclic mobility. These results emphasize the critical role of shallow soil layers in controlling seismic response when deeper strata are modeled as purely elastic.

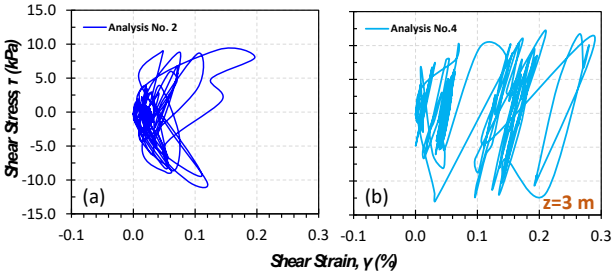


Figure 8. Shear stress-strain results obtained from NL analyses with constant modulus and damping ratio below 20 m depth

Figure 9 presents a comparative evaluation of the constitutive and pore pressure generation models in terms of excess pore water pressure development during strong ground shaking. The figure shows that Analysis No. 2 exhibits the most rapid increase in excess pore pressure, reaching full liquefaction conditions ($r_u \approx 1$) around 50 seconds, suggesting a highly contractive response under dynamic loading. Similarly, Analysis No. 1 approaches $r_u=1$ shortly afterward, though with a more gradual rise. In contrast, Analyses No. 3, 4, and 5 display slower pore pressure accumulation, indicating more dilative or less contractive behavior of the respective soil models. Among these, Analysis No. 5 demonstrates the most stable response, with $r_u$ remaining below 0.8 throughout the shaking period. These differences highlight the significant influence of both the selected constitutive model and the pore pressure generation mechanism on the predicted liquefaction potential and dynamic response of the soil.

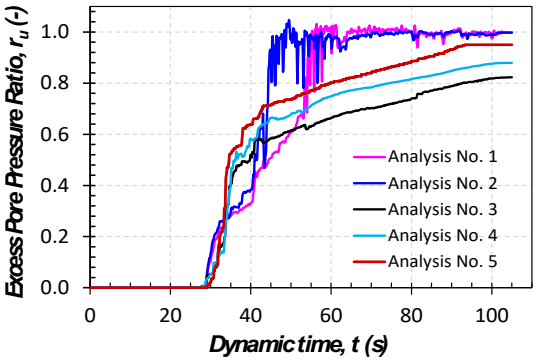


Figure 9. Comparison of excess pore water pressure ratio obtained from analyses during shaking

Figure 10 presents the spectral acceleration–period relationships derived from the analyses at the foundation level (z = 3 m), juxtaposed with the input motion spectrum applied at the model base. The pronounced de-amplification observed in the short-period range (T < 0.5 s) signifies substantial soil softening attributable to the development of excess pore pressure. This phenomenon is most pronounced in Analyses No. 1 and 2, which exhibited the most significant spectral reductions, aligning with the onset of liquefaction. The concurrent spectral elongation towards longer periods further indicates the degradation of shear stiffness and the nonlinear response of the soil. Conversely, Analysis No. 5 exhibited minimal spectral change, suggesting a more stable and less contractive soil behavior under seismic loading. These spectral trends are consistent with the excess pore pressure ratios obtained in previous analyses, thereby corroborating the reliability of model-based liquefaction detection. Overall, spectral acceleration analysis proves to be an effective tool for identifying dynamic manifestations of liquefaction in saturated alluvial Gölbaşı soils.

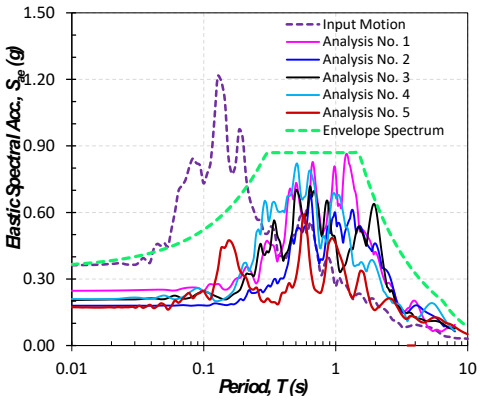


Figure 10. Comparison of spectral acceleration with period obtained from analyses and envelope spectrum

## 5 CONCLUSIONS

This study presents a comparative evaluation of pore pressure generation and liquefaction constitutive models implemented in widely used geotechnical analysis platforms, based on a real soil profile characterized through laboratory and in-situ investigations conducted in Gölbaşı district of Adıyaman province, where severe liquefaction-induced damage was observed during the Türkiye February 6, Kahramanmaraş Earthquakes. From the obtained results, the following conclusions can be drawn:

- Field and laboratory investigations conducted in the Gölbaşı district revealed that, within the upper 20 meters, liquefiable thick silty sand alluvial layers are interbedded with low-plasticity silty and sandy clays.
- In order to account for liquefaction effects in one-dimensional site response analyses, the liquefiable layers within the upper 20 meters were calibrated using pore water pressure generation models available in the DeepSoil software, based on results from consolidated undrained cyclic direct simple shear (CDSS) tests. Accordingly, pore pressure model parameters were proposed specifically for the silty sand and low-plasticity silty clay layers identified in the Gölbaşı site.
- Similar calibrations were also performed in the finite element software Plaxis 2D for the embedded PM4Sand and PM4Silt constitutive models, based on the results of consolidated undrained cyclic direct simple shear (CDSS) tests. The PM4Sand model was employed for silty sand layers, while the PM4Silt model was used for low-plasticity silty clayey units. For soils encountered below a depth of 20 meters, material behavior was defined using the HSSmall model and linear elastic properties based on shear wave velocity.
- Based on the results of in-situ SPT tests, constitutive parameters for the UBC3D-PLM model were defined for the silty sand layers. Accordingly, a series of site response analyses were conducted incorporating five different constitutive models and assumptions. In all analyses, a ground motion record was selected from a station located near the Gölbaşı district and matched to the shear wave velocity profile of the site under investigation.
- Significant shear strains and excess pore pressure ratios approaching unity were observed within the upper 5 meters of the soil profile, indicating a high potential for liquefaction or cyclic mobility. The considerable

development of excess pore water pressure under seismic loading implies a substantial reduction in effective stress, potentially leading to strength loss and stiffness degradation in shallow soil layers. Additionally, amplified peak horizontal accelerations in the upper strata underscore the influence of soft soils on seismic wave amplification.

- The evolution of excess pore pressure varies notably with the choice of constitutive and non-liquefiable layer models. Analyses incorporating the PM4Sand/PM4Silt models with advanced formulations such as HSSmall (Analysis 1) or using MRD-based pore pressure generation (Analysis 5) reached ru ≈ 1, indicating full liquefaction. In contrast, analyses using Linear Elastic models for non-liquefiable layers (Analyses 2 and 4) showed slower pore pressure buildup, reflecting reduced stress redistribution and drainage effects.

- The spectral acceleration response is significantly affected by both the choice of constitutive model and the representation of non-liquefiable layers. Analyses utilizing more sophisticated soil models, such as HSSmall (Analyses 1 and 3), demonstrate relatively higher amplification in the short to intermediate period range (T ≈ 0.2–1.0 s), effectively capturing the nonlinear response of soft soils. Conversely, Analysis 5 (DeepSoil), which employs MRD-based modulus reduction and damping (MRD) curves within a simplified nonlinear framework, exhibits comparatively lower amplification, particularly in the short-period range. This is likely attributable to the limited stress-strain nonlinearity and the absence of advanced stiffness degradation modeling.

## 6 ACKNOWLEDGEMENTS

This study was supported by the Scientific and Technological Research Council of Turkey (TÜBİTAK) under the 1001 Research Program, Project No. 123M604.

## REFERENCES

AFAD. (2025). Turkish Accelerometric Database and Analysis System (TADAS). Retrieved from Disaster and Emergency Management Authority: https://tadas.afad.gov.tr

Akıl, B. et al., 2008. Evaluation of Settlement Suitability of Gölbaşı (Adıyaman) Town, located on the East Anatolian Fault Zone. Türkiye Jeoloji Bülteni, 51(1), pp. 43-57 (In Turkish).

Arpat, E., & Şaroğlu, F. (1972). THE EAST ANATOLIAN FAULT SYSTEM; THOUGHTS ON ITS DEVELOPMENT.

Bentley(2025), PLAXIS2D V24 Material Models Manual 2D.

Boulanger, R. W. and Idriss, I. M. (2014). CPT and SPT based liquefaction triggering procedures. Report No. UCD/CGM-14/01. University of California, Davis: Center for Geotechnical Modelling.

Boulanger, R. W., & Ziotopoulou, K. (2023a). PM4SAND (VERSION 3.3): A SAND PLASTICITY MODEL FOR EARTHQUAKE ENGINEERING APPLICATIONS.

Boulanger, R. W., & Ziotopoulou, K. (2023b). PM4SILT (VERSION 2.1): A SILT PLASTICITY MODEL FOR EARTHQUAKE ENGINEERING APPLICATIONS.

Bozbey, I. et al., (2023). Development of an analytical approach for the prediction of liquefaction-induced foundation damage in shallow-foundation buildings on silty-clay alluvium soils considering building characteristics and neighboring building interaction Adıyaman-Gölbaşı Case, Ankara: TUBİTAK.

Cabalar, A. F., Canbolat, A., Akbulut, N., Tercan, S. H., & Isik, H. (2019). Soil liquefaction potential in Kahramanmaras, Turkey. Geomatics, Natural Hazards and Risk, 10(1), 1822–1838. https://doi.org/10.1080/19475705.2019.1629106

Çetin, K. Ö., Elsaid, A., & Ozacar, A. (2025). Intensity Characteristics of Seismograms Recorded During the February 6, 2023, M7.8 Türkiye Kahramanmaraş Pazarcik Earthquake. Turkish Journal of Civil Engineering, 36(2), 29–51. https://doi.org/10.18400/tjce.1348206

Darendeli, M. B. (2001). Development of a new family of normalized modulus reduction and material damping curves Ph.D. Dissertation, University of Texas at Austin, TX

Flora, A., Bilotta, E., Valtucci, F., Fierro, T., Perez, R., Santucci de Magistris, F., Modoni, G., Spacagna, R., Kelesoglu, M. K., Sargin, S., Altinok, E., Oztoprak, S., Bozbey, I., & Aysal, N. (2024). Liquefaction effects in the city of Gölbaşı: from the analysis of predisposing factors to damage survey. Engineering Geology, 338,107633.https://doi.org/https://doi.org/10.1016/j.enggeo.2024.107633

Gokceoglu, C., Cetin, K. O., Kayen, R. E., & Crosta, G. (2024). Preface: Engineering Geology – Volume 341. Engineering Geology, 341, 107702. Elsevier. https://doi.org/10.1016/j.enggeo.2024.107702

Hashash, Y. M. A., Musgrove, M. I., Harmon, J. A., Ilhan, O., Xing, G., Numanoglu, O., Groholski, D., Phillips, C. A., & Park, D. (2020). DEEPSOIL V7.0, User Manual. Board of Trustees of University of Illinois at Urbana-Champaign.

Makra, A. (2013). EVALUATION OF THE UBC3D-PLM CONSTITUTIVE MODEL FOR PREDICTION OF EARTHQUAKE INDUCED LIQUEFACTION ON EMBANKMENT DAMS Msc Graduation Thesis.

Matasovic, N. (1993). Seismic response of composite horizontally-layered soil deposits Ph.D. Dissertation, University of California, Los Angeles

Matasovic, N., & Vucetic, M. (1995). Generalized Cyclic-Degradation-Pore-Pressure Generation Model for Clays. Journal of Geotechnical Engineering, 121, 33-42. doi:10.1061/(ASCE)0733-9410(1995)121:1(33)

Menq, F. Y. (2003). Dynamic properties of sandy and gravelly soils Ph.D. Dissertation, University of Texas at Austin, TX

Milev, N., Takashi, K., Briones, J., Briones, O., Cinicioglu, O., & Torisu, S. (2024). LIQUEFACTION-INDUCED DAMAGE IN THE CITIES OF ISKENDERUN AND GOLBASI AFTER THE 2023 TURKEY EARTHQUAKE. Archives for Technical Sciences, 1(30). https://doi.org/10.59456/afts.2024.1630.079m

Öser, C., Sarğin, S., Yildirim, A. K., Korkmaz, G., Altinok, E., & Kelesoglu, M. K. (2025). Geotechnical aspects and site investigations on Kahramanmaras earthquakes, February 06, 2023. Natural Hazards, 121(5), 5637–5668. https://doi.org/10.1007/s11069-024-07028-8

Özden, G., & Kartal, B. (2025). Seismic Response of Saturated Soils in Gölbaşı District of Adıyaman Province to February 06, 2023 Kahramanmaraş Earthquake. Dokuz Eylül Üniversitesi Mühendislik Fakültesi Fen ve Mühendislik Dergisi, 27(80), 160–169. https://doi.org/10.21205/deufmd.2025278001

Robertson, P. K. (2009). Interpretation of cone penetration tests — a unified approach. Canadian Geotechnical Journal, 46(11), 1337–1355. https://doi.org/10.1139/T09-065

Sahin, A., & Onder Cetin, K. (2024). Liquefaction at two petrochemical facilities during the February 6, 2023, Kahramanmaras-Turkiye earthquake sequence. Engineering Geology, 335, 107539. https://doi.org/https://doi.org/10.1016/j.enggeo.2024.107539

Sandıkçıoğlu, M., Uzun, A., Sol, B., & Sabancı, S. (2023). 6 Şubat 2023 Kahramanmaraş depremlerinin Gölbaşı Havzası'nda sebep olduğu yüzey deformasyonları ve yerleşmeler üzerindeki etkileri, Adıyaman/ Türkiye. Türk Coğrafya Dergisi, 83, 87–99. https://doi.org/10.17211/tcd.1342050

Seed, R. B., et al. (2003). Recent advances in soil liquefaction engineering: A unified consistent framework. Berkely, California: Earthquake Engineering Research Institute.

Tonyalı, İ., Akbas, S. O., Beyaz, T., Kayabalı, K., & Gokceoglu, C. (2024). Case study of a foundation failure induced by cyclic softening of clay during the 2023 Kahramanmaraş earthquakes. Engineering Geology, 332, 107477. https://doi.org.10.1016/j.enggeo.2024.107477

Tsuchida, H. (1970) Prediction and Countermeasure against Liquefaction in Sand Deposits. In: The Seminar of the Port and Harbour Research Institute, 1-33.